THE JOURNAL OF PHYSICAL CHEMISTRY B

Article

pubs.acs.org/JPCB

Ultrafast Proton Dynamics in Aqueous Amino Acid Solutions Studied by Resonant Inelastic Soft X-ray Scattering

M. Blum,[†,‡,§] M. Odelius,[∥] L. Weinhardt,*[,†,§,⊥] S. Pookpanratana,[†] M. Bär,[†,#,○] Y. Zhang,[†] O. Fuchs,[§] W. Yang,[‡] E. Umbach,[△] and C. Heske*[,†,⊥,□,●]

[†]Department of Chemistry, University of Nevada, Las Vegas, Nevada, United States

[‡]Advanced Light Source, Lawrence Berkeley National Laboratory, Berkeley, California, United States

[§]Experimentelle Physik VII, Universität Würzburg, Würzburg, Germany

[∥]Fysikum, Albanova University Center, Stockholm University, Stockholm, Sweden

[⊥]Institute for Photon Science and Synchrotron Radiation, [△]Karlsruhe Institute of Technology, Karlsruhe, Germany

[#]Solar Energy Research, Helmholtz-Zentrum Berlin für Materialien und Energie GmbH, Berlin, Germany

[○]Brandenburgische Technische Universität, Cottbus, Germany

[□]Institute for Chemical Technology and Polymer Chemistry, Karlsruhe Institute of Technology, Karlsruhe, Germany

[●]ANKA Synchrotron Radiation Facility, Karlsruhe Institute of Technology, Karlsruhe, Germany

ABSTRACT: Resonant inelastic soft X-ray scattering (RIXS) has been used to study the electronic structure of glycine and lysine in aqueous solution. Upon variation of the pH value of the solution from acidic to basic, major changes of the nitrogen K edge RIXS data are observed for both amino acids, which are associated with the protonation and deprotonation of the amino groups. The experimental results are compared with simulations based on density functional theory, yielding a detailed understanding of the spectral changes, as well as insights into the ultrafast proton dynamics in the intermediate core-excited/ionized state of the RIXS process.

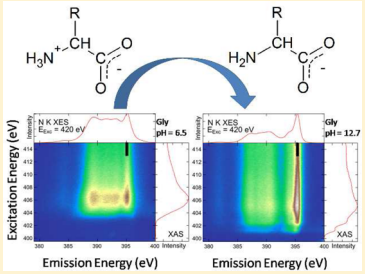

INTRODUCTION

The 20 naturally occurring amino acids are the building blocks of most biologically relevant macromolecules.[1] In acidic aqueous solution, all amino acids exist as a cation, that is, their amino group is protonated, while the carboxylic group is neutral. For a basic solution, the carboxylic and amino groups are both deprotonated (the former being negatively charged and the latter being neutral), and thus, the amino acid acts as an anion. For intermediate pH values, amino acids form a zwitterionic state in which both the carboxylic group and the amino group are charged, forming an overall charge-neutral state. This strong pH dependence of the amino acid is reflected in the behavior of peptides and proteins and, thus, in the strong dependence of their biological activity in different pH environments. To study the impact of such pH variations on the local electronic structure of the amino acid molecule *in solution*, we have used resonant inelastic soft X-ray scattering (RIXS) at the nitrogen K edge to elucidate the electronic and chemical properties of two selected amino acids, glycine and lysine.

In the past, the electronic structure of amino acids has mainly been investigated by soft X-ray spectroscopy of the solid state[2−26] or the gas phase.[11,27−34] For the latter, the amino acid is always neutral and the zwitterionic state does not occur,[35] whereas the solid state is zwitterionic,[36] unless other charges are deliberately introduced into the crystal structure.[22] Of highest interest, however, are insights gained from amino acids in their native biological environment, that is, in aqueous solution, where their net charge depends on the pH value, as described above. Only due to technical developments in the very recent past, it is now possible to perform pH-dependent soft X-ray spectroscopy of solutions, for example, using X-ray absorption spectroscopy (XAS) or X-ray photoelectron spectroscopy (XPS) on liquid jets.[37−41] Using X-ray emission spectroscopy (XES) in a liquid cell, a pioneering study of glycine solutions was published by Gråsjö et al.[42] In addition to presenting the variations of electronic structure at the O K and N K edges as a function of pH, they also briefly speculate that the shape of the XES spectra and, thus, the electronic structure for different pH values are influenced by ultrafast nuclear rearrangements. Recently, we have published a N K edge RIXS study on ammonia in liquid water,[43] where we find evidence for ultrafast molecular dissociation.

To gain further insights into the role of such dynamical properties upon N 1s core hole ionization in the case of amino acids, this present work reports on a combined experimental and theoretical study using RIXS maps, which include XES and XAS information and ground state and dynamical density

Received: March 28, 2012
Revised: October 19, 2012
Published: October 29, 2012

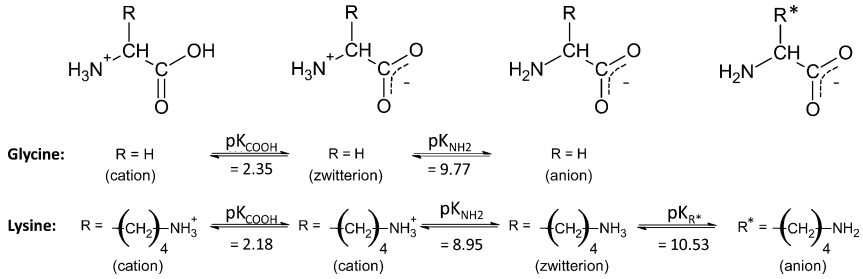

Figure 1. (Top) General Lewis structure of an amino acid as a function of pH value. *R* indicates a rest group specific for each amino acid. (Center) *R* for the amino acid glycine, with corresponding pK_α values. (Bottom) *R* for the amino acid lysine, with corresponding pK_α values.

functional theory. In this study, we primarily focus on glycine and use lysine for comparison to aid in the interpretation of the observed spectral features.

Glycine (NH_2-CH_2-COOH) is the smallest amino acid, consisting only of an amino (α-amino) and a carboxylic functional group. Lysine, in contrast, exhibits two different amino groups: the main α-amino group and the *n*-butylamine side chain. The Lewis structures of the two amino acids are shown in Figure 1. The different forms of the amino acid in solution (cation, anion, and zwitterion) are determined by the pH and pK_a values (with *a* = COOH, NH_2, or R*),[44] as also shown in Figure 1. At the isoelectric point ($pI_{glycine}$ = 6.06, pI_{lysine} = 9.82), the number of deprotonated carboxylic groups (COO^-) equals the number of protonated amino groups (NH_3^+), and thus, the molecule is in the zwitterionic state [note that, for lysine, the zwitterionic state is an intermediate state: only the α-amino group is protonated (NH_3^+) and the *n*-butylamine side chain is deprotonated (NH_2)]. For very high pH values (above the pK_{NH_2} value of 9.77 for glycine and above the pK_{R*} value of 10.53 for lysine), the uncharged amino groups are dominant, while, for low pH values (below the pK_{COOH} value of 2.35 for glycine and 2.18 for lysine), the carboxylic group is (predominantly) uncharged.[44]

METHODS

Experimental Section. Nitrogen K edge RIXS maps and nonresonant XES spectra of glycine and lysine in aqueous solution were recorded using the SALSA (solid and liquid spectroscopic analysis) endstation[45] at the roll-up position of beamline 8.0.1 at the Advanced Light Source, Lawrence Berkeley National Laboratory. SALSA houses a custom-designed flow-through liquid cell (3.6 μL), in which the cell content is continuously renewed ~20 times per second to avoid an influence of beam damage effects on the spectra of the solution under study. The liquid is separated from the ultrahigh vacuum of the SALSA endstation by a 150 nm thick, nitrogen-free SiC window membrane (NTT). Emitted photons are detected with a high-resolution, high-transmission soft X-ray spectrometer with an entranced slitless design, a spherical collecting mirror, a variable line spacing grating, and a soft X-ray CCD.[46] The data is presented as a RIXS map, that is, a two-dimensional representation of the color-coded emission intensity as a function of emission (abscissa) and excitation (ordinate) energy (see Figure 2, which will be discussed below).

Half-saturated aqueous solutions of DL-glycine (12.5 g/100 mL; i.e., 33 water molecules per 1 glycine molecule) and DL-lysine (15 g/100 mL; i.e., 54 water molecules per 1 lysine molecule) from Sigma Aldrich (99.8%) were prepared with ultrapure water (Sigma Aldrich). We used pH values of 1.5, 6.5, and 12.7 for glycine and 5.1, 9.3, and 13.4 for lysine. The pH values at room temperature were adjusted either by adding sodium hydroxide pellets (≥98%, Sigma Aldrich) or aqueous HCl (50%, Alfa Aesar) and controlled by a pH meter equipped with a BlueLine electrode from Schott that was calibrated with pH = 4.0, 7.0, and 10.0 buffer solutions.

Theoretical. The solvation of glycine at different pH values was modeled by hydration clusters, in which nine water molecules were included to solvate the functional groups of the glycine molecule. The hydrated glycine had five accepting hydrogen bonds around the COOH group and one accepting and two donating hydrogen bonds around the NH_2 group. The zwitterion had a similar hydrogen bond configuration, except that the NH_3^+ group did not accept any hydrogen bond. Both, geometry optimizations and X-ray spectrum simulations, were carried out using density functional theory (DFT) in the StoBe-deMon code[47] on the level of gradient-corrected exchange and correlation functionals.[48,49] All atoms were described with double-ζ valence basis sets, including polarization functions,[50] except for the core-excited nitrogen atom, which is described using a flexible IGLO basis set.[51] The simulated XES spectra are based on Kohn–Sham eigenstates from electronic ground-state calculations (i.e., not taking excited-state effects into account), which has been shown earlier to give a good representation for X-ray emission spectra of glycine.[8] Neglecting the dynamic response in the excited state, the XES spectra are calculated for the ground-state geometry. However, due to the finite lifetime of the core-excited state, the system has time to evolve the nuclear motion under the influence of strong forces experienced in the core-excited/ionized state. Therefore, it can be important to include the effects of core-excited/ionized state dynamics in N 1s XES spectra. This is done by sampling the X-ray emission along classical trajectories in the core-ionized state, assuming an exponential lifetime decay.[52−54] Quantum effects that influence the spectral profile have been neglected, but in the present case the forces in the core-hole states are sufficiently large to assume that the classical approximation captures the qualitative effects in the spectra. We assume a lifetime of 5.7 fs for the core-excited state based on values obtained for N_2[55] and for NH_3.[56] To display the calculation on a common energy scale with the experimental data, a constant offset was added to the energy position of the orbitals, such that the calculated highest occupied molecular orbital (HOMO) for R-NH_2 fits the position of the corresponding experimental peak. To describe the experimental broadening, the orbitals were convoluted with a Gaussian with a full-width-at-half-maximum (fwhm) of 0.4 eV (i.e., the spectrometer was operated with an energy resolution $E/\Delta E$ of ≈1000). A convolution of the calculated spectrum

dx.doi.org/10.1021/jp302958j | J. Phys. Chem. B 2012, 116, 13757−13764

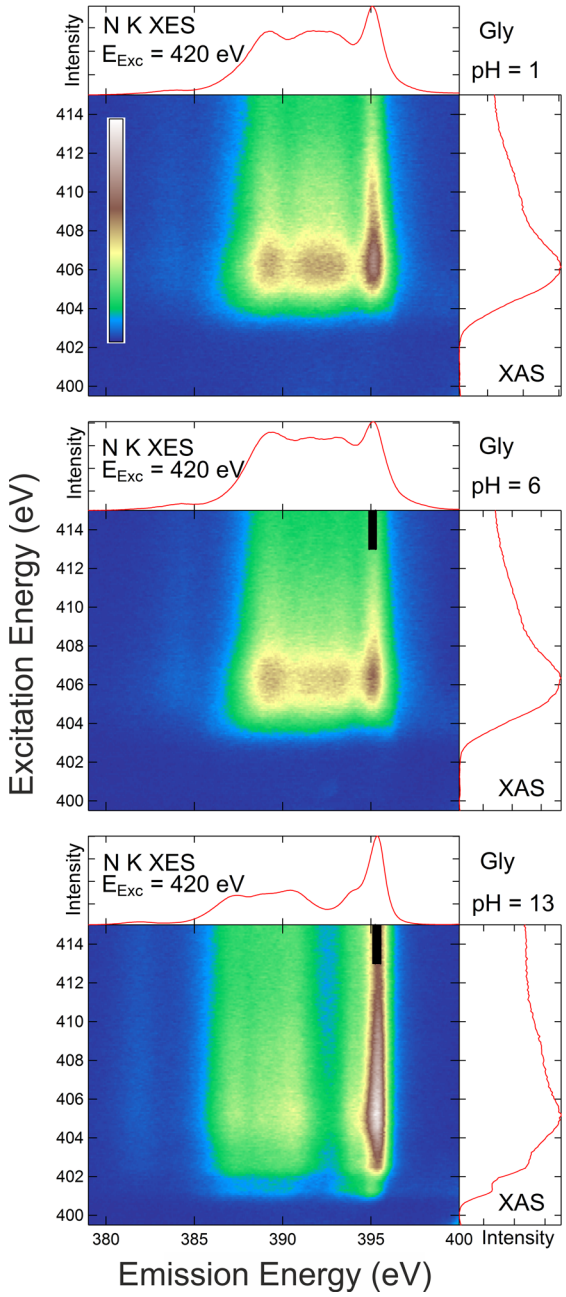

Figure 2. N K RIXS maps of aqueous glycine solutions with pH = 1.5 (top), pH = 6.5 (center), and pH = 12.7 (bottom). Nonresonant XES spectra (excitation energy E_{exc} = 420 eV) and PFY XAS spectra (emission energy integrated over 379−400 eV) are shown above and on the right of each RIXS map, respectively. Black bars at the top of the pH = 6.5 and 12.7 maps (at ca. 395 eV emission energy) indicate the emission energy integration region for the spectra shown in Figure 5.

with suitable Lorentzian functions was also included to account for lifetime, vibrational, and other broadenings. The Lorentzian width for the ground state DFT calculations was varied continuously between 2.5 eV (at 387.3 eV emission energy) and 0.7 eV (at 395.5 eV emission energy) to model the differences in the width of the vibrational envelope for orbitals with bonding (broader and at lower emission energies) and nonbonding (narrower and at higher emission energies) character. The chosen widths lead to best agreement with the experimental data. Note that vibrational envelopes often exhibit asymmetric line shapes; however, to reduce the number of parameters needed for the broadening of the calculated spectra and to account for the fact that a large number of vibrational modes needs to be superposed, we have simply employed a symmetric Lorentzian line shape. The same broadening scheme was used for deriving XES spectra from the dynamical calculation.

RESULTS AND DISCUSSION

Figure 2 shows the N K RIXS maps of the aqueous glycine solutions with pH = 1.5 (top), 6.5 (center), and 12.7 (bottom). As mentioned above, the maps are functions of emission and excitation energy and the RIXS intensity is color-coded. A horizontal cut through these maps corresponds to an emission spectrum for a particular excitation energy, normalized to the excitation intensity. The top of each RIXS map shows a nonresonant XES spectrum (excitation energy of 420 eV), while partial fluorescence yield (PFY) XAS spectra are shown at the right-hand side of the maps (integrating over an emission energy range of 379−400 eV). These XAS spectra are in very good agreement with previous XAS studies of glycine solutions of different pH values by Messer et al.[37,38] For example, the main resonances are observed at ∼405 eV (pH = 12.7) and ∼406 eV (pH = 1.5 and 6.5), respectively. This resonance has been assigned to N 1s → σ^* transitions.[38] In addition, the XAS spectrum of the pH = 12.7 solution reveals two pre-edge features at 401.3 and 402.5 eV, which have also been assigned to 1s → σ^* transitions ($\sigma^*_{NH_2}$ and σ^*_{NH}).[38] Thus, the particular features in the N 1s XAS spectrum in both cases correspond to states with strongly N−H antibonding character.

All three nonresonant XES spectra (pH = 1.5, 6.5, and 12.7) show a maximum at ∼395 eV (the maximum for pH = 12.7 is shifted to higher emission energy by 0.3 eV) and broader features between 385 and 395 eV. The intensity maximum at 395 eV is most dominant for the pH = 12.7 spectrum, while a broad feature between 390 and 394 eV, as well as a second distinct peak at 389 eV, is found for pH = 1.5 and 6.5. The findings for pH = 6.5 and 12.7 are in good agreement with the recently published data by Gråsjö et al. (data for the N K edge around pH = 1.5 was not reported).[42]

A closer look at the resonant portion of the RIXS maps reveals that the overall emission structure is preserved throughout the resonant excitation regime, but that variations in width and relative intensities can be observed as the excitation energy is varied. This is most clearly seen in the pH = 1.5 and 6.5 maps, in which the overall width of the valence state emission is broader for excitation energies at the absorption onset (which will be discussed later). In the following, we will limit our discussion to the pH = 6.5 and 12.7 maps. In principle, no variations are expected between the pH = 1.5 and 6.5 N K RIXS maps, because the probed nitrogen atoms are nominally in the same chemical state. However, as is evident from both the nonresonant XES spectrum as well as the resonant behavior in the RIXS map, we find some differences in the relative intensities of the various orbital contributions to the emission spectrum. While the origin of these differences is presently not understood, we speculate that it either could be related to the high concentration of Cl^- ions stemming from the HCl used to adjust the pH value in the pH = 1.5 solution or a slightly changed charge distribution around the nitrogen atom caused by the deprotonation of the carboxyl group, in

dx.doi.org/10.1021/jp302958j | J. Phys. Chem. B 2012, 116, 13757−13764

accordance with the explanation of a small shift of the N 1s photoelectron line in ref 41.

For a first approximative understanding of the XES spectra, we analyze the electronic structure of glycine in its electronic ground-state geometry. The different pH conditions are modeled by microsolvated clusters of either a single deprotonated (pH = 12.7) glycinate ion or a glycine zwitterion (pH = 6.5). The dipole transition matrix elements between the occupied molecular orbitals of the full system and the N 1s orbital are derived from an electronic ground state (GS) DFT calculation. The magnitude of the matrix elements, as well as the relative energies of the occupied molecular orbitals (after aligning the dominant line with the experimental spectrum), is shown in the bottom panel of Figure 3 (denoted as "GS Calc."). To allow better comparison with experiment, the lines derived from the GS DFT matrix element analysis were convoluted with Gaussian and Lorentzian profiles to include experimental, vibrational, and lifetime broadening, as specified in the previous section. The result is shown in Figure 3 (red spectrum) together with the experimental data (green). As can be seen, the calculated spectrum for the glycinate ion (NH_2) is in good agreement with the experiment, despite the approximate treatment of the X-ray emission process. Only the region between 387 and 393 eV appears compressed in the calculations compared to the experimental spectrum. The same calculations were performed for a glycine molecule in the zwitterionic state (pH = 6.5) surrounded by water molecules. The result (red), together with the experimental data (green), is shown in the center of Figure 3. In contrast to pH = 12.7, the GS calculation for pH = 6.5 does not agree well with experiment. The experimental spectrum shows highest intensity for the high-energy peak at 395.1 eV, which is very weak in the calculated spectrum. Good agreement is only achieved at the low-energy side of the spectrum. To obtain a better description, calculations that include dynamical effects were performed for the models of pH = 6.5 and 12.7.

For low pH values, the calculations show that the -NH_3^+ group undergoes ultrafast dissociation in the core-ionized state. In this process, the hydrogen-bonded N−H bonds are initially elongated (+ 0.3 Å after 5 fs), and then a proton is detached within 10−20 fs, forming an -NH_2 group. For high pH-values, the core-excitation has a less dramatic influence on the -NH_2 group. Initially, the asymmetric N−H stretch is vibrationally excited (ΔN−H = 0.04 Å after 5 fs). Subsequently, intermolecular degrees of freedom are affected: 10−20 fs after excitation, the donating hydrogen bonds are shortened and the accepting hydrogen bonds are broken by reorientation of the water molecule that is H-bonded to the nitrogen lone-pair. The maps in Figure 2 reveal that the high-energy peak is present for all excitation energies, suggesting that the dissociation does not only take place for core-ionized, but also for core-exited states (the excitation-energy dependence will be discussed in more detail below).

In Figure 3, lifetime averages of dynamically calculated XES spectra along the core-ionized state trajectories are shown (in blue, "Dyn. Calc.") above the experimental spectrum in each case. These lifetime averages correspond to a weighted sum of the "snapshot" spectra (see Figure 6, discussed below) after different times using an exponential decay and a core-hole lifetime of 5.7 fs. In accordance to the dynamical effects discussed above, their inclusion has a negligible influence on the spectra at pH = 12.7. At pH = 6.5, however, the dynamical calculation shows a pronounced intensity at ∼395 eV. The intensity observed at this energy in the experimental data of the pH = 6.5 solution can thus be attributed to proton dynamics. In

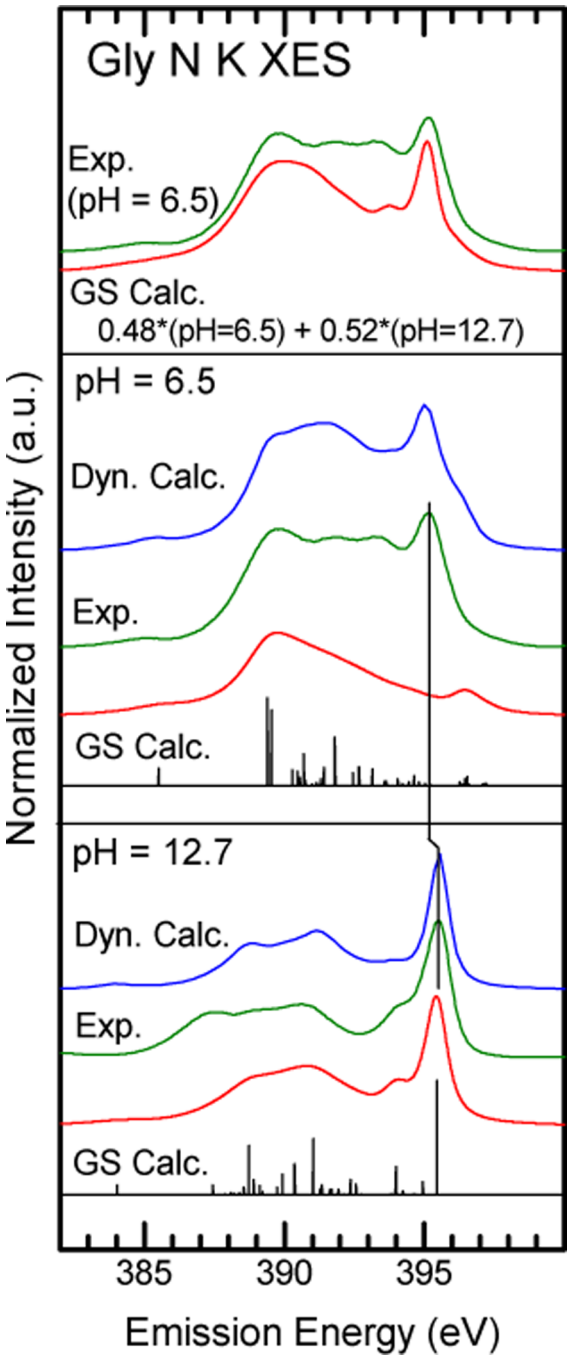

Figure 3. Experimental and calculated nonresonant N K XES spectra of glycine. Bottom (pH = 12.7): ground state (GS) DFT calculation (black), with experimental and lifetime broadening (red), experimental data from Figure 2 (green), and dynamical DFT calculation (blue). The energy scale of the calculation was adjusted to align the prominent peak (at ∼395.5 eV) with the experiment. Center (pH = 6.5): GS calculation (black), with experimental and lifetime broadening (red), experimental data from Figure 2 (green), and dynamical DFT calculation (blue). The energy scale of both calculations is identical to that of the calculation in the bottom panel. The vertical line indicates a shift (of 0.3 eV) of the prominent peak in the experimental spectra. Top: weighted sum of the pH = 6.5 (48%) and pH = 12.7 (52%, shifted by 0.3 eV) GS calculations (red), compared with experimental data for pH = 6.5 (green).

dx.doi.org/10.1021/jp302958j | J. Phys. Chem. B 2012, 116, 13757−13764

a rough approximation, the experimental spectrum can then be described by a weighted sum of the calculated dissociated spectrum, that is, with an NH_2 group, and the undissociated spectrum, that is, with an NH_3^+ group. Note that a similar dissociation process is controversially discussed in the case of liquid water, where the nonresonant O K XES spectrum was described as a superposition of a dissociated and an undissociated component.[54,57−62] To illustrate this model, the top part of Figure 3 shows a spectral sum (GS Calc., red) for which 48% of the calculated spectrum at pH = 6.5 was added to 52% of the calculated pH = 12.7 spectrum. As can be seen in comparison with the experimental data of pH = 6.5 (green), the sum reproduces the dominant peaks at approximately 389 and 395 eV (note that the calculated spectrum for pH = 12.7 was shifted by 0.3 eV to lower emission energy to account for the experimentally observed shift). This supports the earlier speculation by Gråsjö et al.[42] that proton dynamics needs to be considered for a correct interpretation of the XES spectrum and is corroborated with our study on ammonia in liquid water.[43] The sum spectrum reproduces the high energy peak at ∼395 eV very well but shows lower emission intensity at ∼393 eV compared to both, the experimental as well as the dynamical calculation spectrum. In the simple classical MD framework, we ascribe this discrepancy to the fact that, in addition to the two end points of a fully protonated and deprotonated state (taken into account here), intermediate states during the excited state dynamics contribute to the correct spectral sum (see also, discussion of Figure 6).

To shed more light on the suggested model of a superposition of different spectral components, one pertaining to the undissociated (ground state) molecule and others pertaining to the various dissociation pathways, a second amino acid (lysine) was experimentally studied in solutions of different pH values as well. Lysine possesses a second amino group, and the zwitterionic state involves a protonated and a neutral amino group (see Figure 1, bottom). The nonresonant XES spectra (normalized to integrated area) of lysine in an aqueous solution for three pH values (pH = 5.1, 9.3, and 13.4) are shown in Figure 4 (bottom). All three spectra of lysine are dominated by a peak at approximately 395 eV and a broad shoulder between 385 and 393 eV. The main difference between the spectra at different pH values is the ratio between these two features: the lower the pH value, the higher the spectral weight of the broad shoulder. We therefore associate intensity in this spectral region with the NH_3^+ component. Because lysine at pH = 13.4 contains two neutral amino groups, the feature at ∼395 eV can again be assigned to the "pure" NH_2 spectrum, similar to the case of glycine at pH = 12.7. We note that, compared to glycine, the contributions to the lysine spectra appear to be broader, giving rise to the broad shoulder instead of a somewhat more structured spectral shape; this might be due to the fact that lysine contains two amino groups with slightly different chemical environments and a significantly larger number of molecular orbitals.

Figure 4 (top) shows differences of the three pH-dependent spectra: all spectra were normalized to the same overall area, and the pH = 13.4 spectrum was subtracted from the pH = 9.3 and 5.1 spectrum, respectively. As a function of decreasing pH value, the difference spectra show a clear shift of spectral weight to lower emission energy, as mentioned, and also to higher emission energy than the prominent peak at 395 eV. This shift to higher emission energy appears to be more pronounced for pH = 9.3 than for pH = 5.1, while the shift to lower emission

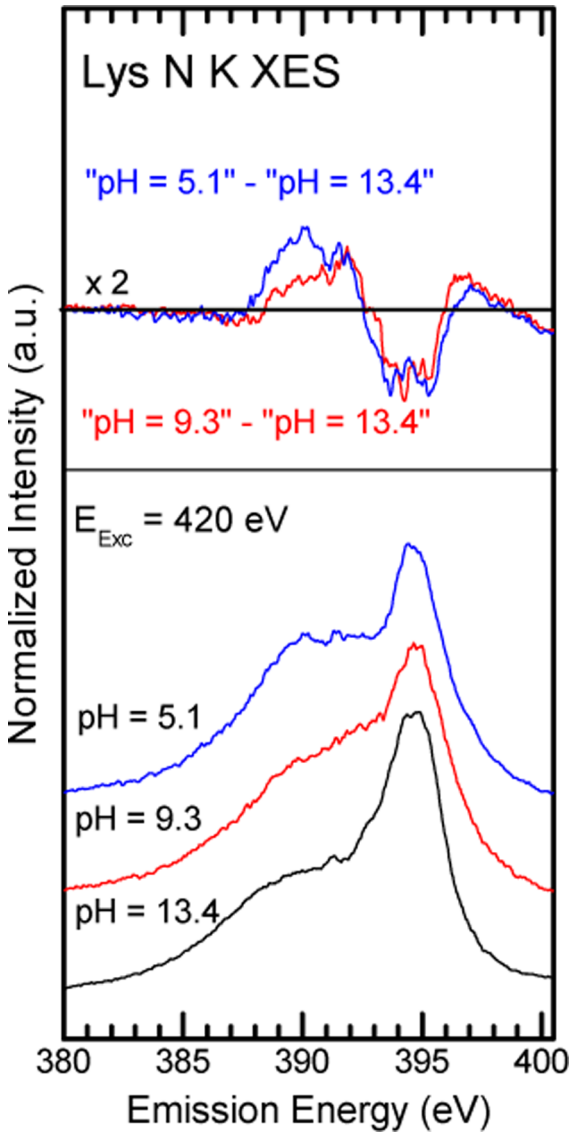

Figure 4. Bottom: Nonresonant N K XES spectra of aqueous lysine solutions with pH = 5.1, 9.3, and 13.4. Spectra were normalized to integrated area. Top: Magnified (×2) difference spectra "pH = 5.1" − "pH = 13.4" and "pH = 9.3" − "pH = 13.4".

energy is most pronounced for pH = 5.1. At present, the origin of the additional intensity at 396 eV for low pH values is unknown, but we note that, for glycine (Figure 3), we observe a similar small spectral weight in the pH = 6.5 calculations at ∼396 eV. This suggests that the spectral weight can be attributed to emission from still-intact NH^+_3 groups, while the overall spectrum is dominated by emission from the NH_2 groups resulting from the ultrafast proton dynamics, as observed and calculated for the N K RIXS spectra of glycine (center frame of Figure 3 and upper panel of Figure 6, see below).

All findings above lead to the conclusion that a characteristic "fingerprint" of the NH_2 component can be found (at ∼395 eV) for all amino acid solutions, even if only protonated NH_3^+ groups exist in the ground-state molecules at that pH value. Apparently, the measurement process itself, that is, excitation and emission, influences the molecule on the time scale of the measurement process even for nonresonant excitation. This time scale is governed by the N 1s core-hole lifetime, and thus,

dx.doi.org/10.1021/jp302958j | J. Phys. Chem. B 2012, 116, 13757−13764

the presence of the NH_2 "fingerprint" component demonstrates the importance of ultrafast proton dynamics to understand RIXS and XES of amino acid molecules in solution.

Closer inspection of the RIXS maps reveals that the contribution of the NH_2 component to the overall spectrum of glycine at pH = 6.5 varies with excitation energy. This, in turn, suggests that the relative importance of the ultrafast dissociation also varies, because different core-excitations induce different nuclear dynamics. Therefore, we have compared integrated slices taken from the pH = 6.5 and 12.7 RIXS maps in Figure 2 to quantify this variation. The black bars at the top of the pH = 6.5 and 12.7 maps in Figure 2 at about 395 eV emission energy indicate the emission energy region that was used to integrate the intensity for decay-channel-specific absorption spectra. The resulting two absorption spectra for the pH = 6.5 and 12.7 RIXS maps are shown in Figure 5 as red lines, in comparison with the respective PFY

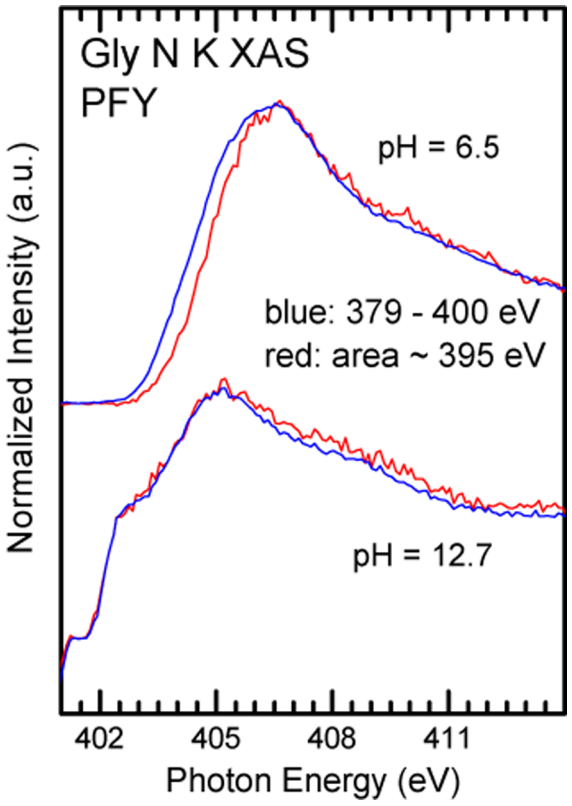

Figure 5. Comparison of decay-channel-specific glycine XAS spectra for pH = 6.5 (red, integrated over emission energies from 394.9 to 395.3 eV) and pH = 12.7 (red, integrated over emission energies from 395.2 to 395.6 eV) with corresponding PFY XAS spectra (blue, integrated over emission energies from 379 to 400 eV).

spectra generated by integrating the emission intensity between 379 and 400 eV, blue lines (also shown at the right-hand side of the maps in Figure 2). In the case of pH = 12.7, the two PFY spectra are identical at the absorption edge. In contrast, there is a noticeable shift of the NH_2 decay-channel-specific spectrum (red) with respect to the PFY spectrum (blue) of pH = 6.5.

This behavior can be understood by considering the duration time of the scattering process. Decreasing the excitation energy below the absorption onset of the pH = 6.5 system also reduces the duration time of the scattering process,[63] and thus, the spectral component indicative of dissociation processes will also decrease. In essence, a resonant excitation below the absorption onset will not give sufficient time for a dissociation of the molecule, and hence, the contribution of dissociation-induced NH_2 species will be smaller than at the absorption resonance and slightly above.

This model is supported by the dynamical DFT calculations in Figure 6. Here, dynamical nonresonant XES snapshot spectra are shown for different time delays after excitation (i.e., core-hole lifetime, ranging from 0 to 8 fs), pH = 12.7 (bottom) and pH = 6.5 (top). For pH = 12.7, spectral changes as a function of time are relatively small, with the most pronounced variation

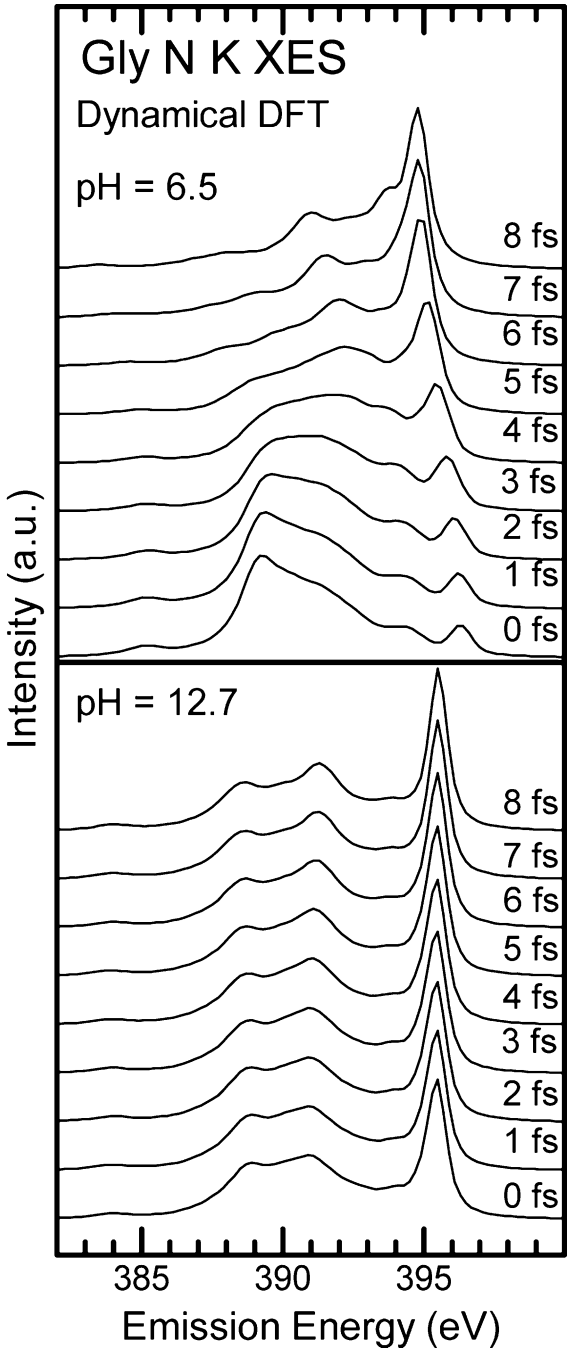

Figure 6. Dynamical DFT calculations of glycine (pH = 6.5 and pH = 12.7), giving "snapshot" emission spectra as a function of core-hole lifetime (0–8 fs). The lifetime averages of these spectra result in the calculated dynamical XES spectra presented in Figure 3.

dx.doi.org/10.1021/jp302958j | J. Phys. Chem. B 2012, 116, 13757–13764

shown by an intensity increase of the peak at 391 eV. The relatively minor changes again indicate the minor influence of dynamical processes on the XES spectra, hence, corroborating that the pH = 12.7 spectrum represents the "pure" NH_2 spectrum. For pH = 6.5, the calculations reveal significant changes as a function of time. In particular, the feature at approximately 395 eV increases in intensity and shifts to lower emission energy as the time delay increases toward the range of, for example, the N 1s core-hole lifetime in N_2 (5.7 fs[55]). Calculated spectra with shorter time delay thus represent spectra with reduced dissociated NH_2 contributions and consequently correspond to experimental XES spectra with excitation energies below the absorption resonance. Furthermore, we noted earlier in the discussion of the pH = 6.5 RIXS map that the overall width of the valence state emission is broader for excitation energies at the absorption onset. This is now reproduced in the dynamical calculation: calculated emission for very short core-hole lifetimes (e.g., 0 fs) spans a much broader range of emission energies than that for very large core-hole lifetimes (e.g., 8 fs). As the detuning below the absorption onset effectively reduces the duration of the scattering process, low-energy excitation portions of the RIXS map are best described by calculated spectra with short core-hole lifetimes, while higher-energy excitations in the RIXS map need to be described by calculated spectra near the actual core-hole lifetime.

CONCLUSIONS

Combining nonresonant XES spectra of lysine and glycine, RIXS maps of glycine, and DFT calculations of glycine at various pH values, we derive the following picture: neutral amino groups (NH_2) in amino acids have a characteristic emission "fingerprint" at approximately 395 eV. While ground state calculations suggest strong spectral changes caused by the change in the local chemical environment at the amino group, this feature can also be found in emission spectra for a pH value at which only protonated amino groups (NH_3^+) should be present. The fact that NH_2-like spectral contributions can be found in these cases suggests the presence of ultrafast dissociation during the N 1s core-hole lifetime. The dissociated spectral fraction decreases by excitation below the first absorption resonance due to shorter duration times of the scattering process. In contrast, the region between 385 and 393 eV of the emission spectra is dominated by the protonated amino groups (NH_3^+), demonstrating the sensitivity of the experimental approach to probe local configurational changes around a selected atom. This shows the strengths of combining the RIXS map concept with suitably designed in situ cells and theoretical spectrum simulations to gain insights into the electronic structure and dynamics of amino acid molecules in a solution environment.

AUTHOR INFORMATION

Corresponding Author

*E-mail: l.weinhardt@kit.edu; heske@unlv.nevada.edu.

Notes

The authors declare no competing financial interest.

ACKNOWLEDGMENTS

The ALS is supported by the Department of Energy, Basic Energy Sciences, Contract No. DE-AC02-05CH11231. M.B. thanks the Helmholtz-Association (VH-NG-423) for support. M.O. acknowledges financial support from the Swedish Research Council (VR), the Carl Trygger Foundation and the Magnus Bergvall foundation, and generous allocations of computer time through SNIC at the Swedish National Supercomputer Center (NSC) and High Performance Computing Center North (HPC2N), Sweden.

REFERENCES

(1) Bryngelson, J. D.; Billings, E. M. *Lect. Notes Phys.* **1997**, *480*, 320−344.
(2) Wu, C. R.; Nilsson, J. O.; Salaneck, W. R. *Phys. Scr.* **1987**, *35*, 586−589.
(3) Bozack, M. J.; Zhou, Y.; Worley, S. D. *J. Chem. Phys.* **1994**, *100*, 8392−8398.
(4) Löfgren, P.; Krozer, A.; Lausmaa, J.; Kasemo, B. *Surf. Sci.* **1997**, *370*, 277−292.
(5) Boese, J.; Osanna, A.; Jacobsen, C.; Kirz, J. *J. Electron Spectrosc. Relat. Phenom.* **1997**, *85*, 9−15.
(6) Hasselström, J.; Karis, O.; Weinelt, M.; Wassdahl, N.; Nilsson, A.; Nyberg, M.; Pettersson, L. G. M.; Samant, M. G.; Stöhr, J. *Surf. Sci.* **1998**, *407*, 221−236.
(7) Hasselström, J.; Karis, O.; Nyberg, M.; Pettersson, L. G. M.; Weinelt, M.; Wassdahl, N.; Nilsson, A. *J. Phys. Chem. B* **2000**, *104*, 11480−11483.
(8) Nyberg, M.; Hasselström, J.; Karis, O.; Wassdahl, N.; Weinelt, M.; Nilsson, A.; Pettersson, L. G. M. *J. Chem. Phys.* **2000**, *112*, 5420−5427.
(9) Tanaka, M.; Nakagawa, K.; Koketsu, T.; Agui, A.; Yokoya, A. *J. Synchrotron Radiat.* **2001**, *8*, 1009−1011.
(10) Kaznacheyev, K.; Osanna, A.; Jacobsen, C.; Plashkevych, O.; Vahtras, O.; Agren, H. *J. Phys. Chem. A* **2002**, *106*, 3153−3168.
(11) Gordon, M. L.; Cooper, G.; Morin, C.; Araki, T.; Turci, C. C.; Kaznacheyev, K.; Hitchcock, A. P. *J. Phys. Chem. A* **2003**, *107*, 6144−6159.
(12) Nyberg, M.; Odelius, M.; Nilsson, A.; Pettersson, L. G. M. *J. Chem. Phys.* **2003**, *119*, 12577−12585.
(13) Tzvetkov, G.; Koller, G.; Zubavichus, Y.; Fuchs, O.; Casu, M. B.; Heske, C.; Umbach, E.; Grunze, M.; Ramsey, M. G.; Netzer, F. P. *Langmuir* **2004**, *20*, 10551−10559.
(14) Cooper, G.; Gordon, M.; Tulumello, D.; Turci, C.; Kaznacheyev, K.; Hitchcock, A. R. *J. Electron Spectrosc. Relat. Phenom.* **2004**, *137*−*140*, 795−799.
(15) Yagi, S.; Matsumura, Y.; Soda, K.; Hashimoto, E.; Taniguchi, M. *Surf. Interface Anal.* **2004**, *36*, 1064−1066.
(16) Zubavichus, Y.; Fuchs, O.; Weinhardt, L.; Heske, C.; Umbach, E.; Denlinger, J. D.; Grunze, M. *Radiat. Res.* **2004**, *161*, 346−358.
(17) Zubavichus, Y.; Zharnikov, M.; Shaporenko, A.; Fuchs, O.; Weinhardt, L.; Heske, C.; Umbach, E.; Denlinger, J. D.; Grunze, M. *J. Phys. Chem. A* **2004**, *108*, 4557−4565.
(18) Zubavichus, Y.; Zharnikov, M.; Schaporenko, A.; Grunze, M. *J. Electron Spectrosc. Relat. Phenom.* **2004**, *134*, 25−33.
(19) Beerbom, M. M.; Gargagliano, R.; Schlaf, R. *Langmuir* **2005**, *21*, 3551−3558.
(20) Zubavichus, Y.; Shaporenko, A.; Grunze, M.; Zharnikov, M. *J. Phys. Chem. A* **2005**, *109*, 6998−7000.
(21) Zubavichus, Y.; Zharnikov, M.; Yang, Y. J.; Fuchs, O.; Heske, C.; Umbach, E.; Tzvetkov, G.; Netzer, F. P.; Grunze, M. *J. Phys. Chem. B* **2005**, *109*, 884−891.
(22) Zubavichus, Y.; Shaporenko, A.; Grunze, M.; Zharnikov, M. *J. Phys. Chem. B* **2006**, *110*, 3420−3427.
(23) Otero, E.; Urquhart, S. G. *J. Phys. Chem. A* **2006**, *110*, 12121−12128.
(24) Zubavichus, Y.; Shaporenko, A.; Grunze, M.; Zharnikov, M. *J. Phys. Chem. B* **2007**, *111*, 9803−9807.
(25) Wilks, R. G.; MacNaughton, J. B.; Kraatz, H.-B.; Regier, T.; Blyth, R. I. R.; Moewes, A. *J. Phys. Chem. A* **2009**, *113*, 5360−5366.
(26) Schwartz, C. P.; Saykally, R. J.; Prendergast, D. *J. Chem. Phys.* **2010**, *133*, 044507−1−6.

(27) Klasinc, L. *J. Electron Spectrosc. Relat. Phenom.* **1976**, *8*, 161−164.
(28) Cannington, P. H.; Ham, N. S. *J. Electron Spectrosc. Relat. Phenom.* **1979**, *15*, 79−82.
(29) Cannington, P. H.; Ham, N. S. *J. Electron Spectrosc. Relat. Phenom.* **1983**, *32*, 139−151.
(30) Slaughter, A. R.; Banna, M. S. *J. Phys. Chem.* **1988**, *92*, 2165−2167.
(31) Powis, I.; Rennie, E. E.; Hergenhahn, U.; Kugeler, O.; Bussy-Socrate, R. *J. Phys. Chem. A* **2003**, *107*, 25−34.
(32) Coutinho, L. H.; Homem, M. G. P.; Cavasso, R. L.; Marinho, R. R. T.; Lago, A. F.; de Souza, G. G. B.; de Brito, A. N.; Brazilian. *J. Phys. (Paris)* **2005**, *35*, 940−944.
(33) Plekan, O.; Feyer, V.; Richter, R.; Coreno, M.; de Simone, M.; Prince, K. C.; Carravetta, V. *J. Phys. Chem. A* **2007**, *111*, 10998−11005.
(34) Plekan, O.; Feyer, V.; Richter, R.; Coreno, M.; de Simone, M.; Prince, K. C.; Carravetta, V. *Chem. Phys. Lett.* **2007**, *442*, 429−433.
(35) Remko, M.; Rode, B. M. *J. Phys. Chem. A* **2006**, *110*, 1960−1967 and references therein..
(36) Jönsson, P.-G.; Kvick, Å. *Acta Crystallogr.* **1972**, *B28*, 1827−1833.
(37) Messer, B. M.; Cappa, C. D.; Smith, J. D.; Wilson, K. R.; Gilles, M. K.; Cohen, R. C.; Saykally, R. J. *J. Phys. Chem. B* **2005**, *109*, 5375−5382.
(38) Messer, B. M.; Cappa, C. D.; Smith, J. D.; Drisdell, W. S.; Schwartz, C. P.; Cohen, R. C.; Saykally, R. J. *J. Phys. Chem. B* **2005**, *109*, 21640−21646.
(39) Nolting, D.; Aziz, E. F.; Ottosson, N.; Faubel, M.; Hertel, I. V.; Winter, B. *J. Am. Chem. Soc.* **2007**, *129*, 14068−14073.
(40) Aziz, E. F.; Ottosson, N.; Eisebitt, S.; Eberhardt, W.; Jagoda-Cwiklik, B.; Vácha, R.; Jungwirth, P.; Winter, B. *J. Phys. Chem. B* **2008**, *112*, 12567−12570.
(41) Ottosson, N.; Børve, K. J.; Spångberg, D.; Bergersen, H.; Sæthre, L. J.; Faubel, M.; Pokapanich, W.; Öhrwall, G.; Björneholm, O.; Winter, B. *J. Am. Chem. Soc.* **2011**, *133*, 3120−3130.
(42) Gråsjö, J.; Andersson, E.; Forsberg, J.; Duda, L.; Henke, E.; Pokapanich, W.; Björneholm, O.; Andersson, J.; Pietzsch, A.; Hennies, F.; et al. *J. Phys. Chem. B* **2009**, *113*, 16002−16006.
(43) Weinhardt, L.; Weigand, M.; Fuchs, O.; Bär, M.; Blum, M.; Denlinger, J. D.; Yang, W.; Reinert, F.; Umbach, E.; Heske, C. *Phys. Rev. B* **2011**, *84*, 104202−1−6.
(44) Nelson, D. L.; Cox, M.M. *Principles of Biochemistry*; Worth Publishers: New York, 2000.
(45) Blum, M.; Weinhardt, L.; Fuchs, O.; Bär, M.; Zhang, Y.; Weigand, M.; Krause, S.; Pookpanratana, S.; Hofmann, T.; Yang, W.; et al. *Rev. Sci. Instrum.* **2009**, *80*, 123102−1−6.
(46) Fuchs, O.; Blum, M.; Weigand, M.; Umbach, E.; Weinhardt, L.; Bär, M.; Heske, C.; Denlinger, J. D.; Chuang, Y.-D.; McKinney, W.; et al. *Rev. Sci. Instrum.* **2009**, *80*, 063103−1−7.
(47) Hermann, K.; Pettersson, L. G. M; Casida, M. E.; Daul, C.; Goursot, A.; Koester, A.; Proynov, E.; A. St-Amant, Salahub, D. R.; Carravetta, V.; et al. *STOBE Software*; 2002.
(48) Perdew, J. P. *Phys. Rev. B* **1986**, *34*, 7406.
(49) Becke, A. D. *Phys. Rev. A* **1988**, *38*, 3098−3100.
(50) Godbout, N.; Salahub, D. R.; Andzelm, J.; Wimmer, E. *Can. J. Chem.* **1992**, *70*, 560−571.
(51) Kutzelnigg, W.; Fleischer, U.; , Schindler, M. *NMR Basic Principles and Progress*; Springer: Heidelberg, 1990; Vol. *23*, p 165.
(52) Brena, B.; Nordlund, D.; Odelius, M.; Ogasawara, H.; Nilsson, A.; Pettersson, L. G. M. *Phys. Rev. Lett.* **2004**, *93*, 148302−1−4.
(53) Odelius, M.; Ogasawara, H.; Nordlund, D.; Fuchs, O.; Weinhardt, L; Maier, F.; Umbach, E.; Heske, C.; Zubavichus, Y.; Grunze, M.; et al. *Phys. Rev. Lett.* **2005**, *94*, 2274011−4.
(54) Odelius, M. *J. Phys. Chem. A* **2009**, *113*, 8176−8181.
(55) Prince, K. C.; Vondráček, M.; Karvonen, J.; Coreno, M.; Camilloni, R.; Avaldi, L.; de Simone, M. *J. Electron Spectrosc. Relat. Phenom.* **1999**, *101−103*, 141−147.
(56) Lindgren, A.; Gisselbrecht, M.; Burmeister, F.; de Brito, A. N.; Kivimäki, A.; Sorensen, S. L. *J. Chem. Phys.* **2005**, *122*, 114306−114314.
(57) Fuchs, O.; Zharnikov, M.; Weinhardt, L.; Blum, M.; Weigand, M.; Zubavichus, Y.; Bär, M.; Maier, F.; Denlinger, J. D.; Heske, C.; et al. *Phys. Rev. Lett.* **2008**, *100*, 027801−1−4.
(58) Fuchs, O.; Maier, F.; Weinhardt, L.; Weigand, M.; Blum, M.; Zharnikov, M.; Denlinger, J. D.; Grunze, M.; Heske, C.; Umbach, E. *Nucl. Instrum. Methods Phys. Res., Sect. A* **2008**, *585*, 172−177.
(59) Fuchs, O.; Zharnikov, M.; Weinhardt, L.; Blum, M.; Weigand, M.; Zubavichus, Y.; Bär, M.; Maier, F.; Denlinger, J. D.; Heske, C.; et al. *Phys. Rev. Lett.* **2008**, *100*, 249802.
(60) Odelius, M. *Phys. Rev. B* **2009**, *79*, 144204−1−6.
(61) Weinhardt, L.; Fuchs, O.; Blum, M.; Bär, M.; Weigand, M.; Denlinger, J. D.; Zubavichus, Y.; Zharnikov, M.; Grunze, M.; Heske, C.; et al. *J. Electron Spectrosc. Relat. Phenom.* **2010**, *177*, 206−211.
(62) Weinhardt, L.; Benkert, A.; Meyer, F.; Blum, M.; Wilks, R. G.; Yang, W.; Bär, M.; Reinert, F.; Heske, C. *J. Chem. Phys.* **2012**, *136*, 144311−144316.
(63) Gel'mukhanov, F.; Ågren, H. *Phys. Rep.* **1999**, *312*, 87−330.